J|A|C|S
ARTICLES
Published on Web 03/13/2004

Faster Dissociation: Measured Rates and Computed Effects on Barriers in Aryl Halide Radical Anions

Norihiko Takeda, Pavel V. Poliakov, Andrew R. Cook, and John R. Miller*

Contribution from the Chemistry Department, Brookhaven National Laboratory, Upton, New York 11973-5000

Received October 9, 2003; E-mail: jrmiller@bnl.gov

Abstract: Carbon−halogen bond dissociation rates for a series of aryl halide radical anions ($ArX^{-\bullet}$: X = Cl, Br) in NMP were measured at room temperature by pulse radiolysis with 10^{-11} s time resolution. To obtain accurate dissociation rates, care was taken to measure and correct for competing decay channels. The observed rates correlated well with activation energies computed in the gas phase by density functional (DFT) calculations. The rates did not correlate well with electron affinities or dissociation energies obtained by the same computational methods, although such correlations are reported in the literature and are expected on the basis of simple models. The calculations also found that the transition state structures had bent carbon−halogen bonds. Bending enables large reductions of the activation energies by an electronic effect involving mixing of π^* and σ^* states. This bending-induced mixing is computed to increase the dissociation rates by a few orders of magnitude and is thus essential to understanding these reactions.

Introduction

Charge transfer to organic molecules can result in scission of chemical bonds.[1] An important class of such reactions is a one-electron reduction of organic halides in solution leading to dissociation of the carbon−halogen (C−X) bond to produce a carbon-centered radical and a halide anion. This reaction has been studied intensely[2−15] because it is a basic element of important chemical processes such as nucleophilic substitution reactions[16] and Grignard reagent formation.[17] Electron attachment to aryl halides usually produces a radical anion intermediate ($ArX^{-\bullet}$), which undergoes C−X bond dissociation as a distinct second step. Upon dissociation, an electron delocalized over π^* orbital is rearranged to be localized on the halogen atom. Substantial information has been gained from gas phase spectroscopy, especially on chlorobenzene and its derivatives,[18,19] and theory has pointed to symmetry requirements that lead to bending of carbon−halogen bonds,[20−22] a theme that will be important here. Rough estimates of dissociation rates are obtained from spectra, and rates have been measured when a bond remote from the center of charge is broken.[23]

In solution dissociation rates of 10^{-2}−10^{8} s^{-1} at room temperature for $ArX^{-\bullet}$ have been measured principally by electrochemical[2−12] and pulse-radiolysis[13−15] techniques. The

(1) Bühler, R. E. In *The Chemistry of the Carbon−Halogen Bond*; Patai, S., Ed.; John Wiley & Sons: London, 1973; Vol. Part 2, pp 795−864. Savéant, J.-M. In *Advances in Physical Organic Chemistry*; Bethell, D., Ed.; Academic Press: London, 1990; Vol. 26, pp 1−130. Savéant, J.-M. *Acc. Chem. Res.* **1993**, *26*, 455−461. Savéant, J.-M. In *Advances in Electron-Transfer Chemistry*; Mariano, P. S., Ed.; JAI Press: London, 1994; Vol. 4, pp 53−116. Maslak, P. *Top. Curr. Chem.* **1993**, *168*, 1−46. Burrow, P. D.; Gallup, G. A.; Fabrikant, I. I.; Jordan, K. D. *Aust. J. Phys.* **1996**, *49*, 403−423. Bietti, M.; Steenken, S. In *Electron Transfer in Chemistry*; Balzani, V., Ed.; Wiley-VCH: Weinheim, Germany, 2001; Vol. 2, pp 494−579.
(2) Andrieux, C. P.; Dumas-Bouchiat, J. M.; Savéant, J.-M. *J. Electroanal. Chem. Interfacial Electrochem.* **1978**, *88*, 43−48.
(3) Andrieux, C. P.; Blocman, C.; Dumas-Bouchiat, J.-M.; Savéant, J.-M. *J. Am. Chem. Soc.* **1979**, *101*, 3431−3441.
(4) Andrieux, C. P.; Blocman, C.; Dumas-Bouchiat, J.-M.; M'Halla, F.; Savéant, J.-M. *J. Am. Chem. Soc.* **1980**, *102*, 3806−3813.
(5) M'Halla, F.; Pinson, J.; Savéant, J.-M. *J. Am. Chem. Soc.* **1980**, *102*, 4120−4127.
(6) Andrieux, C. P.; Savéant, J.-M.; Zann, D. *Nouv. J. Chim.* **1984**, *8*, 107−116.
(7) Andrieux, C. P.; Savéant, J.-M.; Su, K. B. *J. Phys. Chem.* **1986**, *90*, 3815−3823.
(8) Andrieux, C. P.; Hapiot, P.; Savéant, J.-M. *J. Phys. Chem.* **1988**, *92*, 5987−5992.
(9) Wipf, D. O.; Wightman, R. W. *J. Phys. Chem.* **1989**, *93*, 4286−4291.
(10) Jaworski, J. S.; Leszczynski, P.; Filipek, S. *J. Electroanal. Chem.* **1997**, *440*, 163−167.
(11) Jaworski, J. S.; Leszczynski, P. *J. Electroanal. Chem.* **1999**, *464*, 259−262.
(12) Enemaerke, R. J.; Christensen, T. B.; Jensen, H.; Daasbjerg, K. *J. Chem. Soc., Perkin Trans. 2* **2001**, 1620−1630.
(13) Behar, D.; Neta, P. *J. Phys. Chem.* **1981**, *85*, 690−693. Neta, P.; Behar, D. *J. Am. Chem. Soc.* **1981**, *103*, 103−106. Behar, D.; Neta, P. *J. Am. Chem. Soc.* **1981**, *103*, 2280−2283.
(14) Kimura, N.; Takamuku, S. *Bull. Chem. Soc. Jpn.* **1986**, *59*, 3653−3654.
(15) Kimura, N.; Takamuku, S. *Radiat. Phys. Chem.* **1987**, *29*, 179−183.
(16) Bunnett, J. F. *Acc. Chem. Res.* **1978**, *11*, 413−420. Bunnett, J. F. *Tetrahedron* **1993**, *49*, 4417−4484. Tilset, M.; Parker, V. D. *Acta Chem. Scand., Ser. B* **1982**, *B36*, 311−315. Costentin, C.; Hapiot, P.; Medebielle, M.; Savéant, J.-M. *J. Am. Chem. Soc.* **1999**, *121*, 4451−4460.
(17) Rogers, H. R.; Hill, C. L.; Fujiwara, Y.; Rogers, R. J.; Mitchell, H. L.; Whitesides, G. M. *J. Am. Chem. Soc.* **1980**, *102*, 217−226. Rogers, H. R.; Rogers, R. J.; Mitchell, H. L.; Whitesides, G. M. *J. Am. Chem. Soc.* **1980**, *102*, 231−238. Walborsky, H. M.; Hamdouchi, C. *J. Am. Chem. Soc.* **1993**, *115*, 6406−6408. Peralez, E.; Negrel, J. C.; Chanon, M. *Tetrahedron* **1995**, *51*, 12601−12610. Chanon, M. *Molecules* **2000**, *5*, 289. Chanon, M. *Acta Chem. Scand.* **1992**, *46*, 695−706. Bodineau, N.; Mattalia, J.-M.; Thimokhin, V.; Handoo, K.; Négrel, J.-C.; Chanon, M. *Org. Lett.* **2000**, *2*, 2303−2306.
(18) Stricklett, K. L.; Chu, S. C.; Burrow, P. D. *Chem. Phys. Lett.* **1986**, *131*, 279−284.
(19) Skalicky, T.; Chollet, C.; Pasquier, N.; Allan, M. *Phys. Chem. Chem. Phys.* **2002**, *4*, 3583−3590.
(20) Clarke, D. D.; Coulson, C. A. *J. Chem. Soc. A* **1969**, 169−172.
(21) Beregovaya, I. V.; Shchegoleva, L. N. *Chem. Phys. Lett.* **2001**, *348*, 501−506.
(22) Fontanesi, C. *THEOCHEM* **1997**, *392*, 87−94.
(23) Pearl, D. M.; Burrow, P. D.; Nash, J. J.; Morrison, H.; Nachtigallova, D.; Jordan, K. D. *J. Phys. Chem.* **1995**, *99*, 12379−12381. Pearl, D. M.; Burrow, P. D.; Nash, J. J.; Morrison, H.; Jordan, K. D. *J. Am. Chem. Soc.* **1993**, *115*, 9876−9877.

Table 1. First Order Dissociation Rate Constants (k_d) for Radical Anions of Aryl Halides in 1-Methyl-2-pyrrolidinone (NMP) at Room Temperature Measured by Pulse Radiolysis

chem name	abbrev	k_d (s^{-1})	method, $\log_{10} k_d$, and comparisons to earlier measurements[a]
2-chlorobiphenyl	2ClB	$(6.7 + 7.3/-4.4) \times 10^{10}$	TD 650, **10.8**
3-chlorobiphenyl	3ClB	7.0×10^5	TD 650, **5.8**, 5.9 H[b]
4-chlorobiphenyl	4ClB	$(4.5 \pm 0.2) \times 10^8$	TD 650, **8.7**, 7.9 H[b]
2-bromobiphenyl	2BrB	$>5 \times 10^{10}$	PP 800, >**10.7**
3-bromobiphenyl	3BrB	$(1.3 \pm 0.1) \times 10^9$	TD 650, **9.1**, 8.0 H[b]
4-bromobiphenyl	4BrB	$(3.2 \pm 1.0) \times 10^{10}$	PP 800, **10.5**
1-chloronaphthalene	1ClN	$(1.6 \pm 0.6) \times 10^7$	TD 800, **7.2**, 6.9 H,[b] 7.4 D,[c] 7.2 D,[d] 7.7 S[e]
2-chloronaphthalene	2ClN	1.5×10^7	TD 800, **7.2**, 6.9 H,[b] 8.0 D[d]
1-bromonaphthalene	1BrN	$(1.0 \pm 0.4) \times 10^{10}$	PP 800, **10.0**, 9.0 D,[c] 7.8 D,[d] 8.5 S,[e] 8.3 S[f]
2-bromonaphthalene	2BrN	$(1.8 \pm 0.4) \times 10^{10}$	PP 800, **10.3**, 8.7 D[c]
1-iodonaphthalene	1IN	$>5 \times 10^{10}$	PP 800, >**10.7**, 10.6 A,[f] 9.2 D,[c] 8.8 S[e]
9-chloroanthracene	9ClA	$<7 \times 10^3$	TD 700, <**3.8**, 5.9 H,[b] 4.4/5.6 A,[h] 2.3 A,[f] 2.2 D,[d] 2.3D,[g] 2.2 S[e]
9-bromoanthracene	9BrA	$(3.8 \pm 0.9) \times 10^5$	TD 700, **5.6**, 6.4 H,[b] 6.3 A,[i,j] 5.2 A,[f] 5.9 D,[k] 6.4 D,[d] 5.8 D,[g], 5.5 S,[e] 4.8 S[f]
9,10-dichloroanthracene	9,10Cl_2A	$<8 \times 10^3$	TD 680, <**3.9**, 5.0/6.0 A,[h] 1.1 D[l]
9,10-dibromoanthracene	9,10Br_2A	$(7.7 \pm 0.5) \times 10^4$	TD 680, **4.9**, 5.4 A,[i,j] 4.5 D[c]

[a] Detection method and monitored wavelength (nm): transient digitizer (TD), pulse-probe (PP), and log of the rate measured here in NMP. Rates from previous work are denoted by solvent (S = DMSO, H = HMPA, A = acetonitrile, D = dimethylformamide). [b] Pulse radiolysis.[15] [c] Electrochemical redox catalysis (ECAT).[12] [d] ECAT.[6] [e] ECAT.[4] [f] Product analysis of deuterium incorporation after electrolysis.[5] [g] Direct electrochemistry (rapid scan).[9] [h] Laser photolysis in the presence of 1 M cation scavenger (amines).[45] [i] Pulse radiolysis.[44] [j] Laser photolysis in the presence of 1 M cation scavenger (amines).[46] [k] Direct electrochemistry (rapid scan).[8] [l] Direct electrochemistry (rapid scan).[11]

rates have been interpreted in the context of energetic data such as electrochemical potentials[6,7,24] and computed driving forces[10,12,25] and are often in good accord with theoretical descriptions.[24] What is missing in this large and elegant body of literature is measurement of rates near 10^9 s^{-1} and faster. In a few cases, rates up to $\sim 5 \times 10^9$ s^{-1} have been reported using indirect methods.[12,26]

This paper describes measurements of such fast dissociation of aryl halides obtained by pulse radiolysis with the new LEAF accelerator facility at Brookhaven National Laboratory. A series of chloro- and bromo-substituted biphenyls, naphthalenes, and anthracenes and 1-iodonaphthalene were each dissolved in 1-methyl-2-pyrrolidinone (NMP, $\epsilon_r = 32.2$) and were subjected to pulse radiolysis at room temperature. First-order dissociation rate constants in the range from $\sim 10^4$ to $\sim 10^{11}$ s^{-1} were observed and compared with thermodynamic quantities obtained by density functional (DFT) calculations. The new data presented here extend the range of known $ArX^{-\bullet}$ dissociation rate constants but present a puzzle: a poor correlation of dissociation rates with computed reaction energetics was observed in contrast to previous reports, while a reasonably good correlation with computed activation energies was found. The computations also indicated bent structures of transition states and point to this established concept as essential to understand these reactions.

Experimental Section

Chemicals. Aryl halides (ArXs) and their nonhalogenated counterparts (ArHs) used in this study were purchased from commercial suppliers. In some cases, biphenyl and naphthalene were either recrystallized from ethanol or zone-refined in ambient air. 9-Chloroanthracene and 9-bromoanthracene were each passed through alumina (Aldrich, activated neutral) using hexane as the eluent and recrystallized from ethanol. 9,10-Dichloroanthracene and 9,10-dibromoanthracene were each recrystallized from ethanol. NMP (Aldrich, biotech grade, 99.5+%) was used as received for pulse-probe experiments and was distilled from sodium benzophenone ketyl at reduced pressure and stored under argon for transient digitizer experiments. Other chemicals were used as received. Abbreviations for each ArX are listed in Table 1.

Pulse Radiolysis. Ionization was created in solutions of the ArXs by 7 ps, 9 MeV, and 5 nC electron pulses from Brookhaven National Laboratory's Laser-Electron Accelerator Facility (LEAF).[27] LEAF is one of a new generation of electron accelerators that employs laser pulses to initiate short pulses of electrons. The laser ejects electrons from a photocathode inside an rf cavity in which intense electric fields accelerate the electrons. LEAF is the first such accelerator designed for chemistry research. In addition to providing short electron pulses, synchronized laser pulses are available for use as optical probes. Transient optical absorption signals up to 0.2 ns time resolution were recorded by a Tektronix 680B or 694C transient digitizer (TD). For TD measurements probe light from a pulsed xenon arc lamp was wavelength-selected with interference filters and measured using a silicon photodiode (EG&G FND-100 or Opto Electronics Limited CD10) or a biplanar phototube (Hamamatsu R1328U or 1193U) to obtain overall system rise times of 2 or 0.2 ns, respectively. Transients were typically averaged over 4−10 shots for each run. Faster time resolution was obtained with a "pulse-probe" (PP) detection system. This is analogous to a laser pump−probe experiment, except instead of optical excitation an electron pulse initiated chemistry. For each electron pulse a 100 fs, 800 nm Ti:Sapphire laser pulse probed the transient absorption at up to 10 ns variable delay. Other probe wavelengths are obtained by frequency doubling to 400 nm or production of variable wavelengths by an optical parametric amplifier (Quantronix Topas). In this study the overall system rise time was ~12 ps with 1 cm optical path length. Shorter 7 ps rise time can be obtained with a 0.5 cm path length, at the expense of smaller signals. A Faraday cup monitored the size of each electron pulse to correct for their fluctuations. Signals were averaged over 10−100 shots per each data point.

For TD experiments, argon-saturated solutions were prepared in 2 cm path length quartz cells. The instrumental response function was determined using an aqueous solution containing 1 M NaOH and 10 vol % methanol. Hydrated electrons produce strong optical absorption and decay little and by a known amount in this solution.[28] Iterative reconvolution of the measured instrumental response was included in

(24) Savéant, J.-M. *J. Phys. Chem.* **1994**, *98*, 3716−3724.
(25) Pierini, A. B.; Duca, J. S., Jr. *J. Chem. Soc., Perkin Trans. 2* **1995**, 1821−1828. Pierini, A. B.; Duca, J. S., Jr.; Vera, D. M. A. *J. Chem. Soc., Perkin Trans. 2* **1999**, 1003−1009.
(26) Tanner, D. D.; Chen, J. J.; Chen, L.; Luelo, C. *J. Am. Chem. Soc.* **1991**, *113*, 8074−8081.
(27) Wishart, J. F. In *Photochemistry and Radiation Chemistry Complementary Methods for the Study of Electron Transfer*; Wishart, J. F., Nocera, D. G., Eds.; American Chemical Society: Washington, DC, 1998; Vol. 254, pp 35−50.
(28) Jonah, C. D.; Hart, E. J.; Matheson, M. S. *J. Phys. Chem.* **1973**, *77*, 1838−1843. Bartels, D. M.; Cook, A. R.; Mudaliar, M.; Jonah, C. D. *J. Phys. Chem. A* **2000**, *104*, 1686−1691.

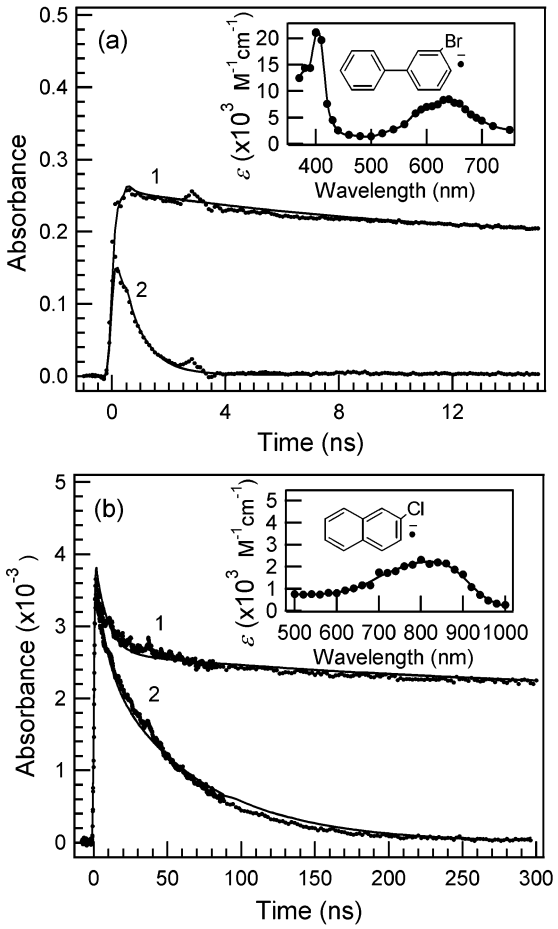

Figure 1. Decay of radical anions of ArH and ArX recorded in transient digitizer experiments with 2 cm optical path length. The solid curves represent kinetic fits. (a) Samples containing 123 mM biphenyl (curve 1) and 150 mM 3-bromobiphenyl (3BrB, curve 2) in NMP. Detection used a biplanar phototube monitoring at 650 nm. (b) Samples containing 100 mM naphthalene (curve 1) and 100 mM 2-chloronaphthalene (2ClN, curve 2) in NMP. Detection at 800 nm used a Si photodiode. Insets: Spectra of $3BrB^{-\bullet}$ and $2ClN^{-\bullet}$ from extrapolation to $t = 0$ of fits such as that shown in curves 2.

the kinetic fits for fast TD decay traces. For PP experiments, samples were prepared under air and transferred into a 1 cm optical path length flow cell. A Gaussian system response function was used during fitting of the PP data. All the measurements were performed at room temperature (20 ± 2 °C).

Molecular Orbital Calculations. Density functional theory (DFT) and Hartree−Fock calculations were performed using the Gaussian 98 package.[29] Molecular structures were visualized using GaussView 3.08 (Gaussian, Inc.). Geometries of molecules were typically fully optimized first by AM1[30] followed by DFT using the B3LYP functional[31] with 3-21G* basis set[32] and then with the 6-31G* basis set.[33] All calculations were spin-unrestricted unless noted otherwise. Starting from the optimized (denoted "OPT") structure obtained for each $ArX^{-\bullet}$, potential energy curves were constructed by changing the C−X distances while relaxing all the other geometric variables at the B3LYP/3-21G* level of theory. Transition state (TS) structures were then optimized at the B3LYP/3-21G* and finally at the 6-31G* level. Zero point energies (ZPEs) were obtained from frequency calculations, which also checked the validity of stationary points. Adiabatic electron affinities of ArX (EA_{ArX}) were estimated from differences in energies between $ArX^{-\bullet}$ and ArX at each optimized geometry. Gas-phase carbon−halogen bond dissociation energies to produce halide ions, $DE_g(ArX^{-\bullet})$, were estimated from energy difference between $ArX^{-\bullet}$ and products (sum of $Ar^{\bullet}$ and X^-) with each geometry optimized. The similar quantity in solution, $\Delta G°(ArX^{-\bullet})$ was computed in single point calculation at the geometries optimized in the gas phase, with the addition of a reaction field of the polarized continuum model (PCM)[34] with $\epsilon = 32.2$ for NMP. Activation energy barriers (E_a) for dissociation of $ArX^{-\bullet}$ were estimated from differences of OPT and TS energies. The reported scaling factor (0.9804) was used when ZPE values (at B3LYP/3-21G* and B3LYP/6-31G*) were included for evaluating electron affinities, dissociation energies, and activation energies.[35]

Results and Discussion

Measurement of Dissociation Rates. Ionization of the solvent (RH) by the electron pulse produces electrons (e^-) and solvent cations ($RH^{+\bullet}$). The electrons are rapidly thermalized and solvated providing a well-defined reducing species (e_s^-), while NMP solvent cations dissociate rapidly to form radicals ($R^{\bullet}$) and solvated protons (RH_2^+). Solvated electrons in NMP have optical absorption in the NIR region ($\lambda_{max} \sim 1600$ nm) with a lifetime of ~ 2 μs[36] and a free electron yield of 102 nmol J^{-1} (G-value = 0.984/100 eV).[37] Solvated electrons, which escape geminate recombination with cations, rapidly attach to solutes and produce their anions. Absorption spectra are known for $ArH^{-\bullet}$ at low temperatures[38−40] and at room temperature[41,42] and have been reported for some $ArX^{-\bullet}$ at low temperature[39,40,43−45] and at room temperature.[15,44−46] Absorption maxima of anions reported here, such as those at ~640 nm for $3BrB^{-\bullet}$ (Figure 1a inset), ~800 nm for $2ClN^{-\bullet}$ (Figure 1b inset), and ~700 nm for $9ClA^{-\bullet}$ (not shown), are in good agreement with those of same aryl moieties previously reported except for broadening relative to spectra at low temperature.

(29) Computations performed with the following: Frisch, M. J.; Trucks, G. W.; Schlegel, H. B.; Scuseria, G. E.; Robb, M. A.; et. al. *Gaussian 98*, revision A.7; Gaussian, Inc.: Pittsburgh, PA, 1998.
(30) Dewar, M. J. S.; Zoebisch, E. G.; Healy, E. F.; Stewart, J. J. P. *J. Am. Chem. Soc.* **1985**, *107*, 3902−3909.
(31) Lee, C.; Yang, W.; Parr, R. G. *Phys. Rev. B* **1988**, *37*, 785−789. Becke, A. D. *J. Chem. Phys.* **1993**, *98*, 5648−5652. Johnson, B. G.; Gill, P. M. W.; Pople, J. A. *J. Chem. Phys.* **1993**, *98*, 5612−5626.
(32) Binkley, J. S.; Pople, J. A.; Hehre, W. J. *J. Am. Chem. Soc.* **1980**, *102*, 939−947. Gordon, M. S.; Binkley, J. S.; Pople, J. A.; Pietro, W. J.; Hehre, W. J. *J. Am. Chem. Soc.* **1982**, *104*, 2797−2803. Pietro, W. J.; Francl, M. M.; Hehre, W. J.; DeFrees, D. J.; Pople, J. A.; Binkley, J. S. *J. Am. Chem. Soc.* **1982**, *104*, 5039−5048.
(33) Hariharan, P. C.; Pople, J. A. *Theor. Chim. Acta* **1973**, *28*, 213−222. Francl, M. M.; Pietro, W. J.; Hehre, W. J.; Binkley, J. S.; Gordon, M. S.; DeFrees, D. J.; Pople, J. A. *J. Chem. Phys.* **1982**, *77*, 3654−3665. Binning, R. C., Jr.; Curtiss, L. A. *J. Comput. Chem.* **1990**, *11*, 1206−1216.
(34) Cammi, R.; Mennucci, B.; Tomasi, J. *J. Phys. Chem. A* **2000**, *104*, 5631−5637. Cossi, M.; Rega, N.; Scalmani, G.; Barone, V. *J. Comput. Chem.* **2003**, *24*, 669−681 and references therein.
(35) Foresman, J. B.; Frisch, A. *Exploring Chemistry with Electronic Structure Methods*, 2nd ed.; Gaussian, Inc.: Pittsburgh, PA, 1996. Wong, M. W. *Chem. Phys. Lett.* **1996**, *256*, 391−399.
(36) Langan, J. R.; Liu, K. J.; Salmon, G. A.; Edwards, P. P.; Ellaboudy, A.; Holton, D. M. *Proc. R. Soc. London, A* **1989**, *421*, 169−178.
(37) Langan, J. R.; Liu, K. J.; Salmon, G. A.; Edwards, P. P. *Proc. R. Soc. London, A* **1989**, *424*, 431−438.
(38) Shida, T.; Iwata, S. *J. Am. Chem. Soc.* **1973**, *95*, 3473−3483.
(39) Arai, S.; Tagawa, S.; Imamura, M. *J. Phys. Chem.* **1974**, *78*, 519−523.
(40) Shida, T. *Electronic Absorption Spectra of Radical Ions*; Elsevier: Amsterdam, 1988; Vol. 34.
(41) Jagur-Grodzinski, J.; Feld, M.; Yang, S. L.; Szwarc, M. *J. Phys. Chem.* **1965**, *69*, 628−635.
(42) Brandes, K. K.; Gerdes, R. J. *J. Phys. Chem.* **1967**, *71*, 508−513.
(43) Namiki, A. *J. Chem. Phys.* **1975**, *62*, 990−998.
(44) Hamanoue, K.; Kimoto, M.; Nakayama, T.; Teranishi, H.; Tagawa, S.; Tabata, Y. *Radiat. Phys. Chem.* **1984**, *24*, 445−448.
(45) Hamanoue, K.; Nakayama, T.; Ikenaga, K.; Ibuki, K. *J. Phys. Chem.* **1992**, *96*, 10297−10302.
(46) Hamanoue, K.; Tai, S.; Hidaka, T.; Nakayama, T.; Kimoto, M.; Teranishi, H. *J. Phys. Chem.* **1984**, *88*, 4380−4384.

Dissociation rates were evaluated using the following scheme:

$$ArX + e_s^- \xrightarrow{k_a} ArX^{-\bullet} \quad (1)$$

$$ArX^{-\bullet} \xrightarrow{k_d} Ar^\bullet + X^- \quad (2)$$

$$ArX^{-\bullet} \xrightarrow{k_3} \text{loss of ions} \quad (3)$$

In the present experiments, electron attachment (reaction 1) produced $10^{-5}-10^{-6}$ M of radical anions on the basis of measurements of biphenyl$^{-\bullet}$ at 650 nm with a well-known extinction coefficient ($\epsilon_{630} = 1.25 \times 10^4$ M^{-1} cm^{-1}).[41] Figure 1 shows representative TD decay data of biphenyl$^{-\bullet}$ and 3BrB$^{-\bullet}$ monitored at 650 nm (panel a) and those of naphthalene$^{-\bullet}$ and 2ClN$^{-\bullet}$ monitored at 800 nm (panel b). Transient absorption signals of ArX$^{-\bullet}$ (curves 2) decay faster than the corresponding ArH$^{-\bullet}$ (curves 1), due to dissociation (reaction 2) and other nondissociative decay processes (reaction 3). The effect of other decay channels described by the sum of two (or sometimes three) exponentials, k_{3a} and k_{3b}, was determined from decay of the appropriate ArH$^{-\bullet}$. Those values were then fixed and included in the fit of ArX$^{-\bullet}$ decays to obtain k_d. This procedure assumes that rates of the nondissociative decay processes are not affected by presence or absence of the halogen, a good assumption when diffusion-controlled reactions such as ion-recombination or rapid reactions with impurities dominate reaction 3. Kinetic fits shown as solid curves in Figure 1 gave $k_d = 1.3 \times 10^9$ s^{-1} for 3BrB$^{-\bullet}$ and $k_d = 1.5 \times 10^7$ s^{-1} for 2ClN$^{-\bullet}$. For fast dissociation reactions the corrections due to nondissociative decay processes are small. They are larger for slow reactions where they become the principal source of uncertainty, such as the very large uncertainty reported for k_d in the slowest, 9ClA$^{-\bullet}$.

To measure dissociation rates k_d it is necessary that the rate of electron attachment (reaction 1) is comparable to or larger than k_d. By monitoring of e_s^- decay at 1000 nm with 0.1−100 mM of solutes, e_s^- attachment rate constants were determined, $k_a = (2-5) \times 10^{10}$ M^{-1} s^{-1}, with halogenated molecules usually near the high end of that range. Thus, to measure a $k_d \geq 10^{10}$ s^{-1} a concentration >0.1 M is needed. Such high concentrations provided another benefit in that some electrons were captured promptly as so-called "dry electrons" reported in water and alcohols.[47] While not observed previously in aprotic solvents, such prompt capture is found here to produce anions without delays required for diffusion of solvated electrons. Prompt or "dry" electron capture was included[48] in the kinetic fits of PP data for ArX$^{-\bullet}$. It occurred to a significant extent only at the high concentrations used in those experiments.

Figure 2 shows examples of PP data monitored at 800 nm in which transient absorption obtained for naphthalene and 1-bromonaphthalene are compared. A portion of absorbance for naphthalene$^{-\bullet}$ decayed in ~100 ps, but the rest stayed almost constant afterward in the time period shown. Most of the fast initial decay is due to geminate ion recombination of anions, but there is some contribution from decay of solvated electrons. Kinetic fits for the 1BrN$^{-\bullet}$ decays shown in Figure 2 along with measurements at different concentrations gave $k_d = (1.0 \pm 0.4) \times 10^{10}$ s^{-1}. The extinction coefficient of 1BrN$^{\bullet-}$ is not necessarily the same as that of naphthalene$^{-\bullet}$ and is therefore not known precisely. In this case data can be fit satisfactorily over a small range of k_d values and extinction coefficients. The uncertainty in the k_d value is principally due to this interplay.

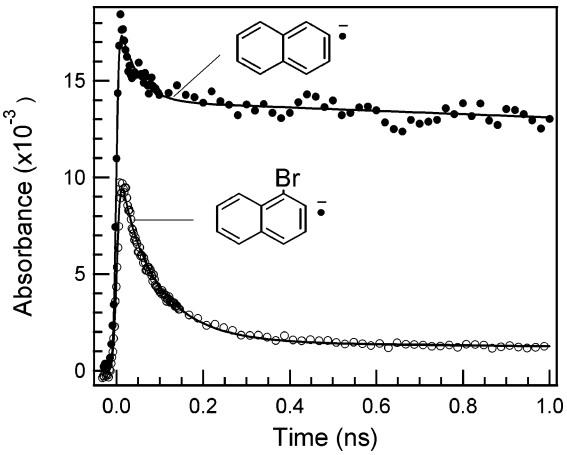

Figure 2. Transient absorption monitored at 800 nm with the pulse-probe radiolysis technique. Optical path length: 1 cm. Samples contained 313 mM naphthalene (●) or 300 mM 1-bromonaphthalene (○) in NMP. Solid curves represent kinetic fits to the experimental data.

In polar solvents such as NMP electrons are known to attach to solutes to form anions without detectable solute cation formation.[36,37] That was usually true in the present work, but in cases where very high (>0.1 M) solute concentrations were used, additional absorptions appeared, most likely due to ArX$^{+\bullet}$ formed by direct ionization. The presence of these cations appeared not to affect the rates of ArX$^{-\bullet}$ dissociation.

For 2-bromobiphenyl and 1-iodonaphthalene only lower limits are reported because no anion was observed, although 2-bromobiphenyl$^{-\bullet}$ has been reported at 100 K.[39] Table 1 gives dissociation rate constants in NMP along with detection methods and monitored wavelengths used to derive k_d.

Comparison to Earlier Measurements. Table 1 also reports comparisons to dissociation rate constants reported previously, where available. Impressive developments in electrochemistry by Savéant and others using competition methods[2−4,7,12,49,50] as well as photolysis[51] have surpassed earlier pulse radiolysis studies to obtain dissociation rates $>10^8$ s^{-1}. The present measurements in NMP ($\epsilon_r = 32.2$) are generally in accord with earlier measurements in DMF ($\epsilon_r = 36.7$) for moderately fast dissociation reactions such as those of 1- and 2-chloronaphthalene anions. But for faster rates such as that for 1BrN$^{-\bullet}$ the 1.0×10^{10} s^{-1} value determined here in NMP is 10−100 times

(47) Aldrich, J. E.; Bronskill, M. J.; Wolff, R. K.; Hunt, J. W. *J. Chem. Phys* **1971**, *55*, 530−539. Jonah, C. D.; Miller, J. R.; Matheson, M. S. *J. Phys. Chem.* **1977**, *81*, 1618−1622. Johnson, D. W.; Salmon, G. A. *J. Chem. Soc., Faraday Trans.* **1978**, *1 74*, 964−974. Lam, K. Y.; Hunt, J. W. *Int. J. Radiat. Phys. Chem.* **1975**, *7*, 317−338. Salter, L. F. *S. Afr. J. Chem.* **1985**, *38*, 87−89. Razem, D.; Hamill, W. H. *J. Phys. Chem.* **1978**, *82*, 1347−1351.

(48) Such processes are exemplified by decrease of initial absorption signal of solvated electrons. The efficiency of "dry" electron capture is expressed using a parameter Q. Survival probability P of presolvated electrons is expressed as $P = \exp(-Qc)$, where c is scavenging solute concentration. The value of $1/Q$ corresponds to C37 concentration of presolvated electron scavenging.

(49) Andrieux, C. P.; Dumas-Bouchiat, J. M.; Savéant, J.-M. *J. Electroanal. Chem. Interfacial Electrochem.* **1978**, *87*, 39−53. Andrieux, C. P.; Dumas-Bouchiat, J. M.; Savéant, J.-M. *J. Electroanal. Chem. Interfacial Electrochem.* **1978**, *87*, 55−65.

(50) Andrieux, C. P.; Hapiot, P.; Savéant, J.-M. *Chem. Rev.* **1990**, *90*, 723−738.

(51) Chesta, C. A.; Cosa, J. J.; Previtali, C. M. *J. Photochem. Photobiol., A* **1988**, *45*, 9−15. Chesta, C. A.; Avila, V.; Soltermann, A. T.; Previtali, C. M.; Cosa, J. J. *J. Chem. Soc., Perkin Trans. 2* **1994**, 2491−2496. Penn, J. H.; Cox, E. D. *J. Org. Chem.* **1986**, *51*, 4447−4449.

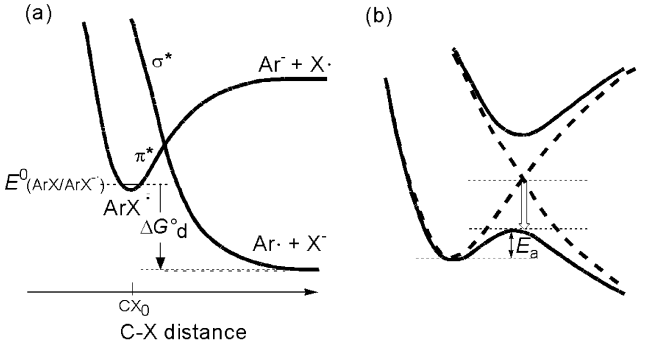

Figure 3. (a) Potential energy diagram for C−X bond dissociation of aryl halide radical anion in solution, reaction 2: $ArX^{-\bullet} \rightarrow Ar^{\bullet} + X^{-}$. The bound diabatic π^* and dissociative σ^* states cross to form an activation barrier. The equilibrium C−X distance (CX_0), the electrochemical potential of ArX/$ArX^{-\bullet}$ couple, $E°(ArX/ArX^{-\bullet})$, and the free energy change of $ArX^{-\bullet}$ dissociation reaction ($\Delta G_d°$) are indicated. (b) The $\pi^*-\sigma^*$ mixing splits the two energy curves (dotted) into adiabatic curves (solid) and reduces the activation energy E_a.

larger than rates determined electrochemically (see Table 1).[4−6,12] The fast electrochemical measurements use the "redox catalysis" method, which relies on kinetic competition from a asymmetric equilibrium to obtain dissociation rates that exceed the apparatus time resolution by several decades.[2,12,49,50] This indirect[2,8,12,50] method obtains rates for dissociation occurring on the nanosecond time scale with instruments having response times of milliseconds or seconds and does so beautifully with the possible exception of rates at the upper end of those reported. Values of k_d determined by the redox catalysis method are strongly dependent on the unknown redox potentials, which must be simultaneously determined along with k_d. A recent paper by Enemærke and co-workers[12] describes improvements to the redox catalysis method. While their reported rate for dissociation of $1BrN^{-\bullet}$ is a factor of 10 smaller than that found here, it is in much better agreement than are values from earlier work (see Table 1), in possible support of their claim.[12] Even with improvements errors may be possible among the faster of the reported rates.[12] In the present pulse-probe measurements there is usually only one unknown,[52] k_d, and all the reported values are within the time constant of the apparatus, so the values reported here are likely to be more reliable. The present data are also in approximate agreement with dissociation rates reported from pulse radiolysis measurements on $3ClB^{-\bullet}$, $1ClN^{-\bullet}$, and $2ClN^{-\bullet}$ in HMPA ($\epsilon_r = 29.6$).[15] Larger discrepancies were found for faster rates such as those for $4ClB^{-\bullet}$ and $3BrB^{-\bullet}$, where about 1 order of magnitude slower rates in HMPA were previously reported.[15]

Energetics of $ArX^{-\bullet}$ Dissociation. Dissociation of molecular ions such as aryl halides is understood in terms of bound π^* and unbound σ^* states (curves in Figure 3a), which cross to form a transition state.[1,20−22,24,25,53,54] When the C−X bond length is at the minimum (CX_o) of the π^* state, if the σ^* state lies higher, as in Figure 3a, then there is an energy barrier and the activation energy for dissociation will be positive.

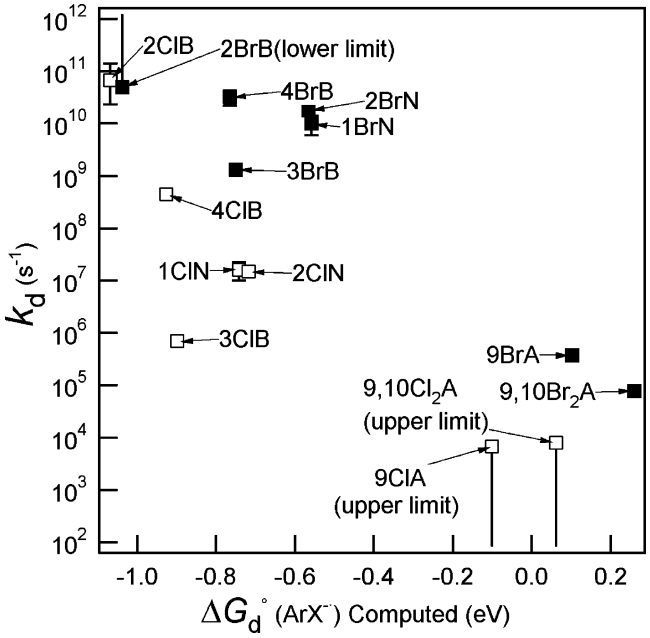

Figure 4. Plots of experimental rate constants (k_d) for dissociation of $ArX^{-\bullet}$ (X = Cl, Br) in NMP measured at room temperature against the computed overall free change for the dissociation reaction, $ArX^{-\bullet} \rightarrow Ar^{\bullet} + X^{-}$. Calculations in NMP are at the B3LYP/6-31G* level with the PCM solvation model.[34]

It is apparent in Figure 3a that the activation energy barrier will be reduced as the overall free energy change of the reaction, $\Delta G_d°$, becomes more negative. This is a typical free energy relation. Such a relationship would be expected to faithfully describe experiment if the shapes of the surfaces (e.g. the $ArX^{-\bullet}$ and $Ar^{\bullet} + X^{-}$ curves in Figure 3) were similar for different reactions having different overall free energy changes. This picture has received support for C−X bond dissociation of $ArX^{-\bullet}$ [12] and C−C bond dissociation of bicumene radical ions.[55] For the present data Figure 4 shows that the dissociation rate constants have only a rough relationship to the dissociation energies, using computed energies in NMP ($\epsilon_r = 32.2$). A corresponding figure using gas-phase energies is in Supporting Information. Strong departures from the notion that rates might correlate with reaction energetics occur for a series of biphenyl and naphthyl halide anions having dissociation rate constants that vary over a range of almost 10^5 although they have similar reaction energetics. Those energetics will be discussed further after referring to a related energy correlation that has been reported in the literature.

The energy of dissociation of an aryl halide anion is expressed in eqs 4a,b for the condensed and gas phase in terms of the energy for dissociation of the carbon−halogen bond in the neutral, ArX, and the difference in redox potentials (or electron affinities) of ArX and $X^{\bullet}$.

$$\Delta G_d°(ArX^{-\bullet}) = \Delta G_d°(ArX) + E°(ArX/ArX^{-\bullet}) - E°(X^{\bullet}/X^{-}) \quad (4a)$$

$$DE_g(ArX^{-\bullet}) = DE_g(ArX) + EA_{ArX} - EA_{X\bullet} \quad (4b)$$

Entropic terms were not included in the gas phase (eq 4b). The last term in eq 4a, the reduction potential of the halogen atom,

(52) For dissociation processes occurring in 100 ps or less there is an analogous uncertainty arising because the extinction coefficient of the radical anion must be simultaneously determined.

(53) Wentworth, W. E.; Becker, R. S.; Tung, R. *J. Phys. Chem.* **1967**, *71*, 1652−1665. Steelhammer, J. C.; Wentworth, W. E. *J. Chem. Phys.* **1969**, *51*, 1802−1814. Burrow, P. D.; Modelli, A.; Chiu, N. S.; Jordan, K. D. *Chem. Phys. Lett.* **1981**, *82*, 270−276.
(54) Laage, D.; Burghardt, I.; Sommerfeld, T.; Hynes, J. T. *Chem. Phys. Chem.* **2003**, *4*, 61−66.
(55) Maslak, P.; Vallombroso, T. M.; Chapman, W. H., Jr.; Narvaez, J. N. *Angew. Chem., Int. Ed. Engl.* **1994**, *33*, 73−75.

Table 2. Computed Electron Affinities of Aryl Halides[a] (EA_{ArX}), C−X Bond Dissociation Energies,[a] $DE_g(ArX^{-\bullet})$, and Activation Energies for Dissociation[a,b] (E_a) of Aryl Halide Radical Anions ($ArX^{-\bullet}$) along with C−X Bond Angles with Respect to Aryl Moieties[c] (∠(Ar−X)) in Optimized (OPT) and Transition State (TS) Geometries[d]

				∠(Ar−X) (deg)		
compd	EA_{ArX} (eV)	$DE_g(ArX^{-\bullet})$ (eV)	E_a (eV)	OPT	TS	$-\Delta E_a$ by bending (eV) (% in parentheses)
2ClB	−0.417	0.188	0.032	8.5	26.8	0.202 (80.2)
3ClB	−0.226	0.534	0.276	0.5	16.7	0.037 (11.6)
4ClB	−0.254	0.523	0.117	0.0	29.7	0.287 (74.3)
2BrB[f]	−0.427	0.215	0.0[g]	11.1	18.1	0.065 (100)
3BrB	−0.203	0.556	0.119	0.8	11.4	0.020 (14.5)
4BrB	−0.221	0.555	0.001	0.0	12.4	0.018 (88.7)
1ClN	−0.231	0.499	0.185	2.5	27.3	0.168 (48.6)
2ClN	−0.224	0.541	0.188	0.4	24.9	0.141 (43.4)
1BrN	−0.204	0.556	0.069	2.7	21.1	0.080 (54.4)
2BrN	−0.196	0.571	0.061	0.3	17.6	0.068 (51.4)
9ClA	0.535	1.221	0.558	0.0	31.2	0.235 (29.5)
9BrA	0.552	1.293	0.411	0.0	29.1	0.186 (31.2)
9,10Cl_2A	0.815	1.476	0.598	0.0	31.5	0.207 (25.6)
9,10Br_2A	0.843	1.551	0.441	0.0	28.7	0.154 (25.7)

[a] Zero point energies (ZPEs) obtained from frequency calculations were scaled by 0.9804. [b] Energy Barriers at 0 K. [c] ∠(Ar−X) defined as the acute angle formed between dissociating C−X bond and diagonal carbons (*para*-position) of aromatic ring. Nonzero values for OPT geometries of naphthalene derivatives are due to in-plane bending. Dihedral angles for corresponding bonds are 0.0°. [d] Also shown is the reduction of energy enabled by C−X bond bending at transition state[e] ($-\Delta E_a$ by bending) for $ArX^{-\bullet}$ anions. All values were computed in gas phase obtained by DFT calculations (B3LYP/6-31G*). [e] Reduction in E_a due to bending, roughly estimated using single point energy calculations for the TS structures with bending angles, ∠(Ar−X), set to the (usually 0) values in the minimized (OPT) structures. ZPE was not included. Values in parentheses are % reduction of the activation energies. [f] Geometries optimized at B3LYP/3-21G* level. [g] No barrier found with 6-31G* basis set.

$E°(X^{\bullet}/X^{-})$, is an important driver of the reaction due to the large electron affinities of $X^{\bullet}$ [56] and strong solvation of X^{-} ions. That term is constant by definition for reactions of a given halide. With one further assumption, that the dissociation energies of neutral aryl halides, $\Delta G_d°(ArX)$, might be approximately constant, then the principle variable in the dissociation energy of aryl halide anions might be the redox potential, $E°(ArX/ArX^{-\bullet})$. Experiments of Savéant and co-workers found a linear relation between log k_d (for $10^{-2} < k_d < 10^8$ s^{-1}) and $E°(ArX/ArX^{-\bullet})$ for series of aryl chlorides and bromides.[6,7,24] This was understood as the nearly linear portion of the parabolic relationship of activation energy to driving force ($\Delta G_d°$).[24] A similar relation was found by Enemaerke.[12] While those correlations had scatter, they were considerably better than that in Figure 4. Although redox potentials are not available for most of the fast-dissociating aryl halides studied here, the relation of rates to redox potentials can be checked using the computed electron affinities (EA_{ArX}) reported in Table 2. Plots of k_d vs EA_{ArX} (Figure S1 in Supporting Information) display the type of scatter seen in Figure 4 for the overall reaction energetics, as do similar plots that include solvation. The correlations in Figures 4 or S1 would be much improved if the dissociation free energy for the slowest member (3ClB) were larger by at least 0.6 eV, and those with intermediate rates were larger increased by correspondingly smaller amounts.

A note of caution is appropriate. An established type of energy correlation is found to fail here, but in the absence of measured energetics, that failure is based on computed energies. The DFT calculations used to establish the *x*-axis of Figure 4 do agree reasonably well with available measured energetics, where available. The computed energies for electron attachment in solution (PCM $\epsilon_r = 32.2$) correlate well with reported redox potentials, where available (see Figure S-4 in the Supporting Information). Solvation energies of X^{-} ions and relative EA's of the $X^{\bullet}$ atoms are in good accord with experiment (see the Appendix). Despite these good indications, it would not be surprising if the calculations had errors of 0.2 eV in the energy changes of one reaction relative to another. On the other hand, much larger errors, arrayed in an improbable way, would be required to provide the cause the departures in Figure 4 and the related plots in the Supporting Information. While experimental measurements and higher levels of calculation are desirable future goals, the failure of rates to correlate with overall energetics appears to be established.

To gain an understanding of this failure, the same electronic structure methods were applied to compute potential energy surfaces.

Computed Potential Energy Surfaces and Activation Energies. Gas-phase potential energy surfaces (PESs) explored along the C−X distance computed by UB3LYP/3-21G* are shown in Figure 5. As the C−X bonds are elongated from their equilibrium lengths, PESs for all $ArX^{-\bullet}$ examined displayed barriers that correspond to transition states (TS). Optimized (OPT) and TS geometries were reoptimized with the 6-31G* basis set, and the activation energies E_a (at 0 K) were estimated except for $2BrB^{-\bullet}$, which had no barrier at the 6-31G* level (Table 2). Stationary points had no imaginary frequencies for minima (OPT) and one for transition states. While the calculations were spin-unrestricted, spin contamination was found to be insignificant ($S^2 = 0.75$). Additional information is provided in the Appendix. The relation of the surfaces to overall energetics needs comment. At C−X distances longer than those shown in Figure 5, the relative energies to OPT state approach the dissociation energies $DE_g(ArX^{-\bullet})$ for the anions shown in Table 2. Although these computed gas-phase DEs are positive (endoergic), the computed reaction energetics become exothermic ($\Delta G_d° < 0$) in solution due to large solvation energies of the halide anions (e.g. Figure 4). Again these calculations appear adequate but may not be highly accurate. Higher levels of calculation, difficult on these molecules, and experiment would be desirable.

Figure 6 shows a good correlation between the measured dissociation rates, k_d, and E_a. The experimental points fall near

(56) NIST, NIST Chemistry Webbook, http://webbook.nist.gov.

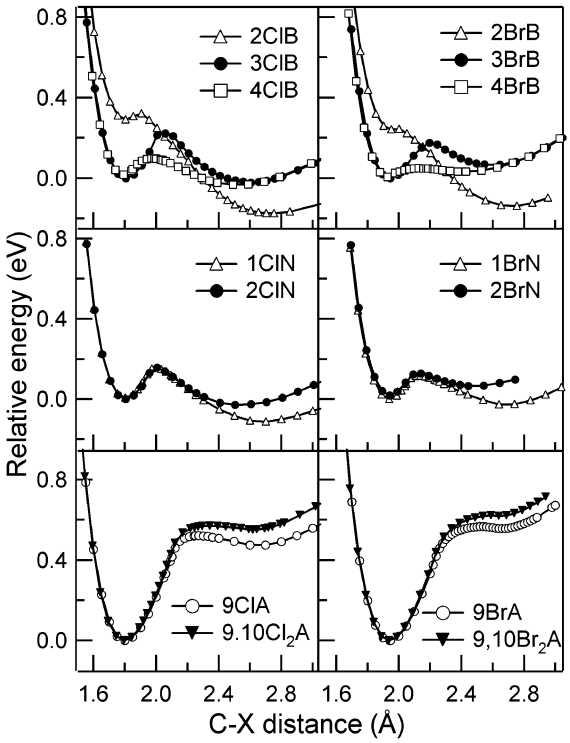

Figure 5. Gas-phase potential energy curves obtained by DFT calculations (B3LYP/3-21G*).

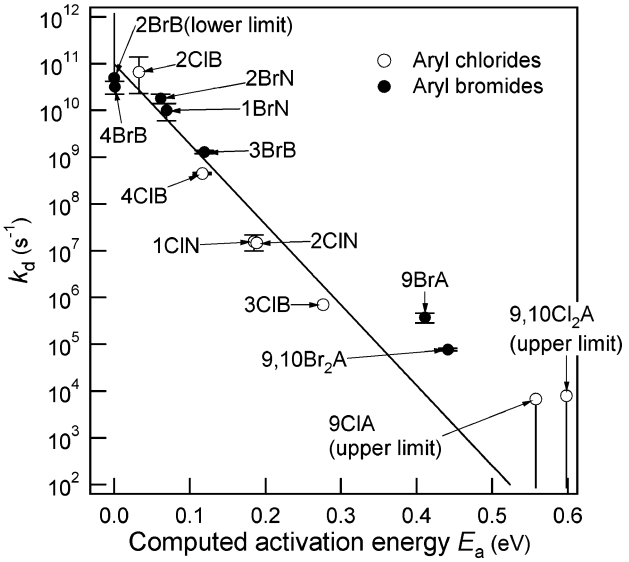

Figure 6. Unimolecular dissociation rate constants (k_d) of aryl halide radical anions in NMP measured at room temperature as a function of activation energies for dissociation (E_a) computed by the DFT method (B3LYP/6-31G*) in the gas phase at 0 K. The solid line represents the equation $k_d = 10^{11} \exp(-E_a/k_BT)$ at $T = 293$ K.

a line having the expected slope (for $T = 293$ K) and a preexponential factor of 10^{11}. The E_as in Figure 6 do not include solvent reorganization, which has been discussed by others,[11,24,54,57] including recent theory by Laage.[58] A figure similar to Figure 6, including *equilibrium* solvation is in the Supporting Information but that will still not account for solvent reorganization. The method used to compute E_a was also used to compute dissociation energies in NMP and electron affinities, so the poor correlations of rates with ΔG_d° (Figure 4) or EA_{ArX} (Supporting Information) are not easily attributed to inadequacies of the computations. While overall reaction energetics characterized by ΔG_d° or $EA(ArX/ArX^{-\bullet})$ do influence rates, a missing factor remains to be identified. This factor will become clear upon examination of the structures of the transition states.

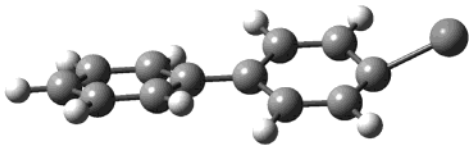

Figure 7. Transition state structure of 4-chlorobiphenyl radical anion computed by DFT at the B3LYP/6-31G* level of theory (gas phase).

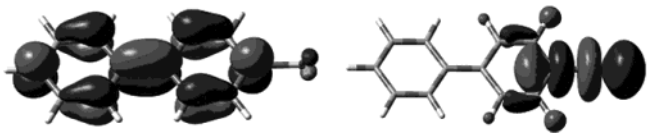

Figure 8. SOMO (left) and LUMO+2 (right) of 4-chlorobiphenyl radical anion computed by DFT at the B3LYP/6-31G* level of theory (gas phase) at isovalue 0.04. The Cl atom is in the plane of the ring to which it is attached. Bending of the C−Cl bond allows mixing of these orbitals.

Bonds Bend Before They Break. In optimized structures of $ArX^{-\bullet}$ the halogen atoms are almost always[59] in-plane with the aryl ring to which they are attached. In contrast the computed TS structures have bent C−X bonds (Table 2), as seen for $4ClB^{-\bullet}$ with a bending angle ∠(Ar−X) of 29.7° (Figure 7). This pattern of a planar anion but a bent transition state is found by DFT at two different basis sets with the present molecules and also in tests on two of the molecules with ROHF method (see the Appendix). Bent TS structures have been reported earlier for related molecules (see the Appendix).[21,25,54]

The bending occurs because it allows mixing of the π^* orbital accommodating unpaired electron with the σ^* orbital on the halogen. The mixing is forbidden by symmetry when the halogen is in-plane, but in the bent structure it provides stabilization. This interaction acts to reduce the energy of the lower, adiabatic surface and, therefore, the activation energy, as illustrated by the solid lines in Figure 3b. Table 2 gives rough estimates of the reductions in E_a due to bending. In the case of $4ClB^{-\bullet}$, the computed reduction is 0.29 eV, increasing the dissociation rate by a factor almost of 10^5. This is the major missing factor responsible for poor correlations of k_d with ΔG_d° and EA_{ArX}. But why does this factor enhance rates for some molecules by several decades and have little effect on others?

The effectiveness of $\pi^*-\sigma^*$ orbital mixing can be qualitatively understood by examining properties of the orbitals involved. Figure 8 pictures the highest occupied orbital, the π-type SOMO of 4-chlorobiphenyl radical anion. At the optimized geometry symmetry prevents mixing of this orbital with the dissociative σ^* LUMO that becomes more localized on the halide as the C−X bond stretches. Out-of-plane bending, such as that in the transition state structure pictured in Figure 7, enables mixing of these two orbitals to stabilize the transition state. In 4-chlorobiphenyl effective mixing is favored by the

(57) Andrieux, C. P.; Savéant, J.-M.; Tallec, A.; Tardivel, R.; Tardy, C. *J. Am. Chem. Soc.* **1996**, *118*, 9788−9789.
(58) Laage, D.; Burghardt, I.; Sommerfeld, T.; Hynes, J. T. *J. Phys. Chem. A* **2003**, *107*, 11271−11291. Burghardt, I.; Laage, D.; Hynes, J. T. *J. Phys. Chem. A* **2003**, *107*, 11292−11306.
(59) Exceptions are the *ortho*-substituted biphenyls (see Table 2). This is probably due to steric repulsions which also increased the Ph−Ph interring angle to ∼25°.

large MO coefficient at the 4(*para*) position. For biphenyl halides the observed dissociation rates for *meta*-isomers were much slower than those for the *ortho* and *para*. This agrees with the larger π^*-SOMO coefficients at the *ortho*- and *para*-positions than the *meta*. SOMOs for all three isomers, pictured in the Supporting Information, are similar in this respect, having nodes very near the *meta* carbon. These dissociations are thus another example of the *ortho*−*para*-directing effect in organic chemistry. The *para* isomers have computed $\Delta G_d°(ArX^{-\bullet})$ almost identical with those of the *meta*, but their activation energies are greatly reduced by bending-induced electronic mixing related to MO coefficients.

A natural question is the following: Why do correlations of rates with overall reaction energetics fail in this study, when they had been reasonably successful in earlier reports? Examination of the rates indicates that the principal source of the present failure is the biphenyls, and the discussion above identifies the nodal properties that are plausibly responsible. LUMOs of the other molecules in this study, halonaphthalenes and -anthracenes, do not have nodes where the halogens are attached. A cursory inspection suggests that this nodal property is usually not found in the ArX molecules in the previous studies in which energy correlations were reported.[6,7,12,24]

Bond bending in dissociation of $ArX^{-\bullet}$ has been discussed in several reports.[6,7,18,19,24,60] An early theoretical paper suggested that symmetry might play a role in $ArX^{-\bullet}$ dissociation reactions,[20] while more recent theoretical papers describe the possible role of bond-bending and the conical nature of the intersections.[21,25,54] Skalicky[19] used gas-phase spectroscopic techniques to show how particular vibrations enhance $\sigma^*-\pi^*$ mixing to increase dissociation yields. This report provides the fastest available measurements of dissociation rate constants. It finds, with the aid of calculations, a reasonably good quantitative description of the experimental observations but only if the effects of bond bending are considered.

The calculations also found that only small changes in C−X bond lengths and charge distributions occurred when going from the equilibrium geometry to the transition state. These results suggest that the effect of solvent polarity on dissociation rates may be small, in contrast to some previous reports.[14,15] Experimental investigation of the effects of solvent polarity as well as more detailed examination of the computations is planned.

Summary and Conclusions

Brookhaven's new LEAF laser-electron accelerator was utilized to study electron attachment and subsequent C−X bond dissociation of halogenated biphenyls, naphthalenes, and anthracenes in the polar organic solvent NMP. Dissociation rates of 10^4 to nearly 10^{11} s^{-1} were measured at room temperature.

Density functional (DFT) calculations were employed to examine thermodynamics of aryl halide radical anions. In contrast to earlier reports, these fast rates did not correlate well with computed reaction energetics but did correlate reasonably well with computed activation energies (E_a) in the gas phase. Examination of the nature of the computed transition state structures obtained by DFT calculations revealed that bending of carbon−halogen bonds yielded large reductions of E_a, which were sometimes computed to be larger than a factor of 10, increasing the rates by as much as 5 orders of magnitude. The modulation of the energy barrier is not dependent on overall energetics but is related to effectiveness of $\pi^*-\sigma^*$ orbital mixing, which, in turn, depends on π^*-orbital coefficients.

In conclusion, this study extended more reliably the measured range of fast dissociation rates for aryl halide radical anions and in addition showed reasonable agreements with results of DFT calculations.

Acknowledgment. This work was supported by the U.S. Department of Energy, Office of Basic Energy Sciences, Division of Chemical Sciences, under Contract DE-AC02-98CH10886. We thank James Wishart and Steve Howell for developments at LEAF and Michel Chanon for alerting us to relevance of fast dissociation rates to Grignard chemistry.

Appendix

In this study, activation energies computed by DFT provided reasonable accounts of experimental results (Figure 6). This Appendix discusses the applicability of those calculations. DFT methods have been shown to predict thermodynamic properties of atoms and molecules. They predict EAs reasonably well,[61] and hybrid DFT methods produce good estimates of electron affinities for anions that are unbound by 1 eV or less and are much better than Hartree−Fock in this respect.[62] Computed EAs for three of the ArX studied here (1ClN, 9ClA, and 9BrA) compare well with known experimental values.[56] B3LYP functionals have been utilized for geometry optimizations of monochlorinated biphenyl anions[63] and to estimate EAs of polychlorinated biphenyls.[64] In Hartree−Fock calculations on chlorotoluene anions[22] spin-contamination in UHF calculations led to a preference for spin-restricted methods. The present DFT calculations performed very well in this respect: Initial values of S^2 were between 0.766 and 0.75 and after projection were 0.75 ± 0.0002. Better electron affinities and the ability to use unrestricted methods with relative freedom from spin contamination support the use of DFT methods.

Figures 6 and S1 (Supporting Information) use B3LYP/6-31G* calculations. Those calculations give underestimates (3.16, 2.84, and −0.24 eV) for the known electron affinities (3.61, 3.36, and 0.28 eV)[56] of Cl and Br atoms and for 1ClN. The relative errors are, however, small. The computed solvation energies in NMP are in very good agreement with those from experiment.[65]

In potential energy surfaces shown in Figure 5, second minima were found at longer C−X distances followed by rising energy. The second energy well is probably due principally to ion−induced-dipole interactions between the aryl radical and

(60) Jordan, K. D.; Burrow, P. D. *Chem. Rev.* **1987**, *87*, 557−558.

(61) Rienstra-Kiracofe, J. C.; Tschumper, G. S.; Schaefer, H. F., III; Nandi, S.; Ellison, G. B. *Chem. Rev.* **2002**, *102*, 231−282. Arulmozhiraja, S.; Fujii, T. *J. Chem. Phys.* **2001**, *115*, 10589−10594. Dessent, C. E. H. *Chem. Phys. Lett.* **2000**, *330*, 180−187.

(62) Szarka, A. Z.; Curtiss, L. A.; Miller, J. R. *Chem. Phys.* **1999**, *246*, 147−155.

(63) Pan, D.; Phillips, D. L. *Chem. Phys. Lett.* **2000**, *318*, 214−221.

(64) Arulmozhiraja, S.; Fujii, T.; Morita, M. *J. Phys. Chem. A* **2002**, *106*, 10590−10595.

(65) The computed ΔG_{solv} in NMP for Cl^- (−2.95 eV) and Br^- (−2.81 eV) agreed reasonably well with the values (−3.07 and −2.95 eV, respectively) deduced from ΔG_{solv} in water and corresponding Gibbs free energy of transfer reported in the literature: Marcus, Y. *Ion Solvation*; John Wiley & Sons: New York, 1985.

the halide ion, an effect discussed by Pause,[66] who described interactions in related radical-ion pairs of magnitudes similar to those found here. The size of ion−induced-dipole interactions is often smaller in other contexts but is aided in the present case by the large polarizabilities of aryl radicals (e.g. 120 bohr^3, isotropic, computed for 4-biphenylyl). There may also be substantial contributions due to artifacts of DFT in dissociation of molecular ions.[67−70] A similar effect appears[22] in MP2 surfaces for 4-chlorotoluene$^{-\bullet}$ but is much smaller on HF surfaces.

Although DFT traces equilibrium regions of PES correctly, in the regions far from equilibrium fractional charges and spin density may be erroneously computed on the fragments.[67] This leads to unphysical results for dissociation of symmetric radical ions such as $H_2^{+\bullet}$ or acetylene dimer cation,[68] and for some types of reactions, DFT was found to underestimate barriers.[69] The origin of the problem has been described,[67] and a criterion for its occurrence is appropriate separation of spin and charge to each fragment.[68] In 4ClB$^{-\bullet}$ at a long C−X distance of 5.5 Å, close to 100% of the negative charge should be localized on Cl, but the present calculations found only 80%. While this is much smaller than the errors in the symmetric systems, there is a problem at long distances.

The transition states found here occur at short distances, 0.2−0.4 Å extension of the C−X bonds, whereas substantial effects of the DFT failure were typically seen at much larger bond extensions.[68] For this reason and because the Ar$^{\bullet}$−X$^-$ pairs do not possess the symmetry that aggravates the DFT problem, it is not likely that the transition states computed here are substantially impacted.

Hartree−Fock results are much less affected, so they provide an additional check that is helpful in indicating whether a significant problem exists. For two of the molecules, 1ClN$^{-\bullet}$ and 4ClB$^{-\bullet}$, ROHF calculations were compared with UB3LYP, both at the 3-21G* level. The results in Table 3 find that the basic features of planar optimized structures and bent transition states were found in ROHF as well as in DFT results, with ROHF giving slightly larger bending in transition states. Activation energies were similar from the two methods for 4ClB$^{-\bullet}$, while ROHF gave a smaller value in 1ClN$^{-\bullet}$. There is no indication that DFT underestimates barrier heights (activation energies) from these comparisons.

Table 3. Comparison of ROHF and DFT (UB3LYP) Methods (3-21G* Basis Set) for Optimized ArX Radical Anions and Their Transition States for Dissociation

		∠(Ar–X)[a] (deg)		
ArX	method	OPT	TS	$E_a^{a,b}$ (eV)
1ClN	ROHF	2.5	39	0.096
	UB3LYP	2.3	26	0.15
4ClB	ROHF	0.0	36	0.08
	UB3LYP	0.0	29	0.08

[a] ∠(Ar−X) at TS and E_a values for ROHF method estimated from the crossing region of PES. [b] Zero point energies were not included in the activation energies.

The question of optimal computational methods for dissociation of ArX$^{-\bullet}$ is far from settled. Methods with extensive CI may help but are difficult on molecules of the size studied here. Benchmarks in the form of experimental measurements of overall energetics are desirable but are not yet available. Electron affinities have been reported for a few of the molecules studied here,[56] but heats of formation of the radicals are not known. The good correlation with experiment found here supports the use of DFT methods, while published calculations[22,25] and results in Table 3 suggest that other methods might perform similarly.

Supporting Information Available: Plots of measured dissociation rates of ArX$^{-\bullet}$ (k_d) against computed electron affinities, gas-phase dissociation energies or activation energies with solvated transition states, comparison of computed and measured redox potentials, and a graphical representation of orbitals for chlorobiphenyl radical anions (PDF). This material is available free of charge via the Internet at http://pubs.acs.org.

JA0389671

(66) Pause, L.; Robert, M.; Savéant, J.-M. *J. Am. Chem. Soc.* **2000**, *122*, 9829−9835. Pause, L.; Robert, M.; Savéant, J.-M. *J. Am. Chem. Soc.* **2001**, *123*, 11908−11916. Cardinale, A.; Isse, A., A.; Gennaro, A.; Robert, M.; Savéant, J.-M. *J. Am. Chem. Soc.* **2002**, *124*, 13533−13539.
(67) Zhang, Y.; Yang, W. *J. Chem. Phys.* **1998**, *109*, 2604−2608.
(68) Bally, T.; Sastry, G. N. *J. Phys. Chem. A* **1997**, *101*, 7923−7925. Hrouda, V.; Roeselova, M.; Bally, T. *J. Phys. Chem. A* **1997**, *101*, 3925−3935.
(69) Glukhovtsev, M. N.; Bach, R. D.; Pross, A.; Radom, L. *Chem. Phys. Lett.* **1996**, *260*, 558−564.
(70) David Sherrill, C.; Lee, M. S.; Head-Gordon, M. *Chem. Phys. Lett.* **1999**, *302*, 425−430.